Reconstruction of zonal precipitation from sparse historical observations using climate model information and statistical learning

Marius Egli[1], Sebastian Sippel[1], Angeline Greene Pendergrass[2], Iris de Vries[1], and Reto Knutti[1]

[1]ETH Zurich
[2]National Center for Atmospheric Research (UCAR)

November 22, 2022

Abstract

Future projected changes in precipitation substantially impact societies worldwide. However, large uncertainties remain due to sparse historical observational coverage, large internal climate variability, and climate model disagreement.
Here, we present a novel reconstruction of large-scale zonal precipitation metrics from sparse rain-gauge data using regularized regression techniques that are trained across climate model simulations.
Subsequently, we test the reconstruction on independent satellite data and reanalyzed precipitation, and find a large fraction of historical zonal mean precipitation variability is recovered, in particular over the Northern hemisphere and in parts of the tropics. Finally, we demonstrate that the reconstructed zonal mean precipitation trends are outside the variability of pre-industrial control simulations, and are consistent with the range of historical simulations driven by external forcing. Overall, we illustrate a novel way of estimating seasonally-averaged zonal precipitation from gauge data, and trends therein that show a signal very likely caused by human influence.

Hosted file

`si_reconstructing_zmp.docx` available at https://authorea.com/users/535235/articles/598696-reconstruction-of-zonal-precipitation-from-sparse-historical-observations-using-climate-model-information-and-statistical-learning

Reconstruction of zonal precipitation from sparse historical observations using climate model information and statistical learning

Marius Egli[1], Sebastian Sippel[1], Angeline G Pendergrass[2,3], Iris de Vries[1], Reto Knutti[1]

[1]Institute for Atmospheric and Climate Science, ETH Zurich, Zurich, Switzerland
[2]Department of Earth and Atmospheric Sciences, Cornell University, Ithaca, NY, USA
[3]National Center for Atmospheric Research, Climate and Global Dynamics Laboratory, Boulder, CO, USA

Key Points:

- Detection and attribution of multi-decadal changes in the water cycle is challenging due to sparse observations, model uncertainty, and internal variability.
- We reconstruct the inter-annual variability of zonal mean precipitation from gauge data using regularized regression techniques.
- We demonstrate that the observed multi-decadal zonal water cycle changes lie within the range of historical climate model simulations.

Corresponding author: Marius Egli, `marius.egli@env.ethz.ch`

Abstract

Future projected changes in precipitation substantially impact societies worldwide. However, large uncertainties remain due to sparse historical observational coverage, large internal climate variability, and climate model disagreement. Here, we present a novel reconstruction of large-scale zonal precipitation metrics from sparse rain-gauge data using regularized regression techniques that are trained across climate model simulations. Subsequently, we test the reconstruction on independent satellite data and reanalyzed precipitation, and find a large fraction of historical zonal mean precipitation variability is recovered, in particular over the Northern hemisphere and in parts of the tropics. Finally, we demonstrate that the reconstructed zonal mean precipitation trends are outside the variability of pre-industrial control simulations, and are consistent with the range of historical simulations driven by external forcing. Overall, we illustrate a novel way of estimating seasonally-averaged zonal precipitation from gauge data, and trends therein that show a signal very likely caused by human influence.

Plain Language Summary

When studying changes in the global water cycle due to climate change it is instructive to study precipitation along constant latitudes (zonal mean), as the average amount and seasonality of precipitation differ strongly across latitudes. When trying to calculate the zonal mean from observations, we face the problem that observations do not exist for many locations at the latitude in question since there may be no precipitation gauges, and the number and locations of gauge stations changes over time. Here we present a method to reconstruct the zonal mean precipitation from spatially incomplete observations, by training a statistical model to predict the zonal mean from only the observed grid cells directly. Our reconstructions show high similarity to satellite-based estimates of zonal mean precipitation. Further, we find a trend in these reconstructions when analyzing the pattern of all zonal trends together, which is very likely caused by human influence.

1 Introduction

Understanding observed historical variability and changes in precipitation on large spatial scales is crucially important for detection of climate change and attribution to human influence in the hydrological cycle, and in order to evaluate and constrain historical and future climate model simulations (Hegerl et al., 2015).

However, understanding historical precipitation variations is challenging because of large internal variability (Deser et al., 2012), and climate model disagreement in the simulation of variability and the response to external forcings (Bindoff et al., 2013). In addition, the observational record is relatively short, often with relatively sparse spatial coverage, in particular prior to the onset of the satellite era, making attribution challenging.

Observations of precipitation, both from rain gauges and from satellites, are used widely to evaluate precipitation trends and variability. Further, these observations are then used to attribute the trends to external forcing and the large-scale modes of internal climate variability. However, the observational record is short and sparse. Precipitation attribution studies are based either on spatially complete but short satellite-based records post-1979 and spatially complete model data (Marvel & Bonfils, 2013), or on longer but spatially incomplete gauge-based observations and climate model output masked to the spatial coverage of the observations (Zhang et al., 2007; Hegerl et al., 2015; Wu et al., 2013). With the latter approach, it was recognized early on that estimates of global or zonal statistics of precipitation from spatially and temporally incomplete observational records with time-varying coverage can lead to biases (Hulme, 1995). In this context, statistical approximations to complement historical records are desirable. Techniques have been developed to fill in missing data and achieve a full coverage field for various climate variables, including temperature or precipitation (Kondrashov & Ghil, 2006; Buttlar et al., 2014; Bárdossy & Pegram, 2014; Coulibaly & Evora, 2007; Kim & Pachepsky, 2010; Chen et al., 2002; Smith et al., 2012). Such reconstruction approaches exist for directly computing large scale metrics such as global mean temperature (Cowtan & Way, 2014; Cowtan et al., 2018) and global mean precipitation (Shen et al., 2014) directly from spatially incomplete data.

More recently, infilling and reconstruction methods have been based not only on statistical relationships or combinations of satellite and *in situ* records, but also combined with information from physical climate models or reanalyses (Kadow et al., 2020). Moreover, recent research has shown that encapsulating information from climate models in statistical models can yield skillful seasonal precipitation forecasts (Gibson et al., 2021). The underlying notion of these approaches is to exploit the large available record of climate model ensemble simulations (Deser et al., 2020) to augment the short and sparse observational record.

The spatio-temporal information provided by climate model simulations has to our knowledge not been systematically exploited for reconstructing large-scale zonal mean precipitation (ZMP) statistics. We thus propose and present a new method for the estimation of ZMP from incomplete gauge data: A statistical regression model trained on climate model data, where each grid cell in the observational coverage mask serves as a predictor for the desired zonal precipitation statistics. Historical observation based zonal-mean precipitation time series can be reconstructed using the statistical model and the observed precipitation record.

In addition to the reconstruction of ZMP, a key interest for detection, attribution and understanding of the historical precipitation record lies in the identification of forced components of precipitation change (Marvel & Bonfils, 2013; Hegerl et al., 2015). While physical understanding provides robust constraints on large-scale precipitation change in a warming climate, such as an increase in global mean precipitation by about 2-3% per degree of warming due to energy balance (Pendergrass & Hartmann, 2014), it is much harder to derive insights on forced changes at regional scales. This is because global mean precipitation is dominated by the tropics and several large regions that show opposite patterns of changes (Muller & O'Gorman, 2011), compensating effects of different external forcing agents (Salzmann, 2016), and large internal variability (Deser et al., 2012; Guo et al., 2019). Studies to date suggest that expected ZMP changes include increasing precipitation in wet mid latitudes and tropics, and persistence and expansion of dry subtropical regions (Held & Soden, 2006; Meehl et al., 2007; Scheff & Frierson, 2012; Berg & McColl, 2021).

Recently, climate model output has been used to train statistical or machine learning techniques to estimate the externally forced response from monthly precipitation maps on a global scale (Barnes et al., 2019; Sippel et al., 2020; De Vries et al., n.d.). ZMP can be a valuable metric to better understand and attribute regional changes in the hydrological cycle with relatively high signal to noise ratio compared to small-scale regional approaches (Marvel & Bonfils, 2013).

Therefore, in the final part of this paper, we will show the long term trends in ZMP reconstructions and compare them to externally forced and unforced climate model projections. We limit the estimation of external influence to an outlook for detection and attribution of ZMP using this approach. Making a comprehensive attribution statement about external influence on ZMP lies outside the scope of this study.

2 Data and Methods

2.1 Observational data and climate model simulations

The precipitation observations for the reconstructions stem from the Global Historical Climatology Network (GHCN) (Menne et al., 2018) as well as from the Global Precipitation Climatology Centre (GPCC) (Schneider et al., 2014). SLP is taken from the 20th Century Reanalysis Project (20CRv3) (Compo et al., 2011; Slivinski et al., 2019). To evaluate our regression-based reconstructions, we use satellite based precipitation data, which is given by the Global Precipitation Climatology Project (GPCP) (Adler et al., 2018). This data set is used entirely as an external source of satellite-based precipitation estimates with global coverage for benchmarking our reconstructions. We compare the reconstructions to the ECMWF reanalysis ERA5 (Hersbach et al., 2020), and a gridded reconstruction of 20th century precipitation provided by Smith et al. (2012), based on principal component regression. Further, we include PREC (Chen et al., 2002), a precipitation reconstruction provided by NOAA, in the comparison.

The climate model data used in this study is obtained from the Large Ensemble Archive (LENS) (Deser et al., 2020). It consists of seven different climate models with a total of 286 ensemble members (See SI, table S1). The climate models are forced with historical greenhouse gas and aerosol concentrations and the data is conservatively regridded onto a 5x5° grid. The variables used are precipitation, surface air temperature and sea level pressure (SLP). We compute the seasonal means for the months December, January and February (DJF) and June, July and August (JJA). We chose these periods since they capture two opposite states of the climate system thus covering a range of processes driving precipitation. We calculate seasonal ZMP for each year and ensemble member for each latitudinal zone of width 5°. To establish a baseline of an unaltered climate the pre-industrial control (piControl) runs from the CMIP5 and CMIP6 archive are used.

2.2 Regularized linear regression for the reconstruction of zonal mean precipitation

We frame the reconstruction problem in the following way: ZMP is a discrete set of time series at varying latitudes. The time series ZMP at a given latitude (lat) can be expressed as a function f of the observed grid cells $\mathbf{X}_{Obs}$ plus a certain error ϵ (Equation 1).

$$ZMP_{lat} = f_{lat}(\mathbf{X}_{Obs}) + \epsilon = \mathbf{X}_{Obs}\beta + \epsilon \tag{1}$$

$\mathbf{X}_{\text{Obs}}$ is a $n \times p$ matrix containing n observations at p locations. We choose f to be a vector β containing p regression coefficients, i.e. ZMP_{lat} is a linear combination of the entries of $\mathbf{X}_{Obs}$. The coefficients are estimated from climate model data, where the predictor matrix is composed of climate models seasonal mean time series reduced (masked) to match the observed locations p (for a given, fixed observational mask) and the target is the "true" seasonal ZMP calculated from the unmasked data. Seasonal mean precipitation, our predictors, is temporally and spatially correlated, which violates one of the criteria for the ordinary least squares (OLS) estimator to be valid, leading to overfitting. To address this we employ a regularized regression technique, often referred to as ridge regression. It imposes a penalty on the magnitude of the coefficients, reducing the degrees of freedom of the regression model. This is achieved via an alteration of the cost function, adding an additional weighted penalty on the sum of squared coefficients (L2-norm) besides the penalty on the sum of squared residuals (RSS) (Eq. 2).

$$argmin\, RSS + \lambda \sum_{j=1}^{p} \beta_j^2 \tag{2}$$

The first term is the cost function of an OLS regression. The second term is referred to as the penalty term where β_j is the j-th of p fitted coefficients. The hyperparameter λ determines the magnitude of the penalty term. For $\lambda > 0$ minimization of this cost function results in smaller coefficients than those obtained with OLS, and coefficients for correlated predictors tend to be evenly distributed between the predictors by nature of the cost function. Thus, when training on spatially correlated climate data, the coefficients are smoothed in space.

2.3 Training procedure for regression models

In order to train the regression models we mask the LENS data such that its coverage includes only those locations for which an uninterrupted observational record from 1950-2014 exists. This allows the use of a single mask for the full time span of a reconstruction.

We use two different reconstruction setups: One based on precipitation data alone, and another which also uses SLP. For the precipitation-only reconstruction setup we mask the training data to represent grid cells for which precipitation observations are available between 1950 and present. Until 1950 station coverage steadily increased, but around 1980 it started to decrease. Using 1950 as a start point means that the reconstruction is less sensitive to low coverage bias than for earlier starting points. As the observational coverage varies in time we use the continuously observed grid cells of a data set. For GHCN this leads to 344 continuous grid cells from 1950-present in GHCN, covering 13% of the entire globe. For GPCC the same criteria yield 467 grid cells. For an overview of the fraction of grid cells containing observations, see figure S1.

The second configuration allows the use of SLP data as predictors in addition to precipitation for the estimation of ZMP. We do not apply a mask for SLP and instead assume that the 20th Century Reanalysis provides reliable seasonal SLP data for the entire observational period of precipitation. This setup is repeated with both precipitation masks for the different precipitation data sets and leads to a regression model with 2936 predictors (344 precipitation + 2592 SLP) for GHCN and 3059 predictors (467 precipitation + 2592 SLP) for GPCC. Thus, the ZMP at a given latitude is calculated in part by precipitation and in part by SLP. The respective weighting is determined via the regression model.

The regression model is trained using the masked climate model data. The training data represents the historical period in the CMIP5 models (1920 to 2005). The target of the regression model is the zonal mean DJF/JJA precipitation. The predictors consist of the masked output of mean DJF/JJA precipitation (and PSL) per grid cell from single ensemble members. Every masked ensemble member is tasked to predict its own unmasked zonal mean precipitation and a model is trained for every latitude individually.

The hyperparameter λ is determined via cross-validation as follows. The training data is split up into groups ("folds") which are successively excluded from the model fit in order to the test regression model's performance on unseen data. In our application, each of the seven models is assigned to one fold each of which is each successively excluded from the fitting process. Subsequently, the root mean squared error (RMSE) for each unseen fold is evaluated and traditionally the λ parameter is chosen to minimize the RMSE. For this study we chose a larger λ resulting in a smaller, more regularized model, which still performs well (Hastie & Qian, 2014). This setup ensures that the regression model does not learn features of a single climate model, thus allowing a better transfer to observations. For an application in a similar context, see Sippel et al. (2020).

3 Results and Discussion

In this section, we first show the regression coefficients of the statistical models (Section 3.1). We evaluate the performance of our ZMP reconstructions across climate models (Section 3.2). Next, we apply the ZMP reconstruction technique to observations, and evaluate the ZMP estimates against satellite data (Section 3.3). Finally, we calculate the trend in the reconstructions and compare the observed zonal trend statistics to forced and unforced climate model simulations (Section 3.4).

3.1 Illustration of regularized regression models

To illustrate the ridge regression technique, we map out the regression coefficients based on their locations, both for a setup based on precipitation alone (Pr) and for a setup that includes precipitation and SLP as predictors (Pr+SLP), for three target latitudes representative for the Southern hemisphere, tropics and Northern hemisphere (Figure 1). In general, positive coefficients are assigned to precipitation grid cells (Pr) at the prediction target's latitude, which implies that local information plays an important role for the respective ZMP. This result is to be expected but also encouraging to see, as the regression model is not given any information about the spatial location of the predictors nor the latitude of the target variable. The precipitation grid cells just north and south of the target latitude tend to be weighted negatively. For example, the model at 47.5°S (Fig. 1a) mainly relies on the few grid cells available in South America and southern Australia, giving positive weights to grid cells close by and negative ones to grid cells further away. For the tropical model (2.5°S) (Fig. 1d) the reconstruction mainly draws from the negative correlation to close-by grid cells north and south, owing to the lack of local grid cells. Positive weights are given to the mid-latitudes. The model for 47.5°N (Fig. 1g) most clearly displays the pattern of having positive weights at the latitude itself and negative ones surrounding it, likely related high local coverage at this latitude.

We next consider the second model setup (Pr+SLP), with spatial patterns of SLP and masked precipitation as joint predictors. As we assume that global-scale SLP variations back to 1950 are reliably reconstructed, we do not mask this data. We first focus on the combined model's precipitation coefficients, shown in the middle row of figure 1. The coefficient patterns are very similar to the ones for the Pr-only setup, especially at 47.5°N (Fig. 1h), where the distribution of the coefficients is hardly distinguishable. The SLP coefficients show negative weights at the predicted zonal band, consistent with low pressure anomalies that are associated with precipitation. The SLP coefficients north and south of the zonal band are positive, reflecting a possible tele-connection pattern in SLP. For all latitudes, SLP predictors receive higher weights in regions where precipitation is not available, thus filling in information in unobserved regions. This can be best seen in the coefficients of the model reconstructing mid latitude northern hemisphere zonal precipitation (47.5 N) (Fig. 1i). Over land, where precipitation grid cells are given to the model, SLP is weighted close to zero. Over the ocean, where no precipitation grid cells are available, SLP is weighted more in comparison. This feature could also occur due to zonal precipitation being dominated by precipitation over the ocean, which the regression model then gravitates to.

3.2 Model-as-truth testing of ZMP reconstruction with climate models

To test how well this method performs for the reconstruction of ZMP, we use a model-as-truth approach, where one climate model is excluded from the training process. The statistical model trained on models except holdout model M is applied to model M. Results from such a reconstruction for two selected latitudes with CESM-CAM5 as left-out model are shown in Fig. 2 (a and d). "Zonal mean Pr" represents the "true" zonal mean precipitation, obtained from the ensemble member's unmasked precipitation data. The

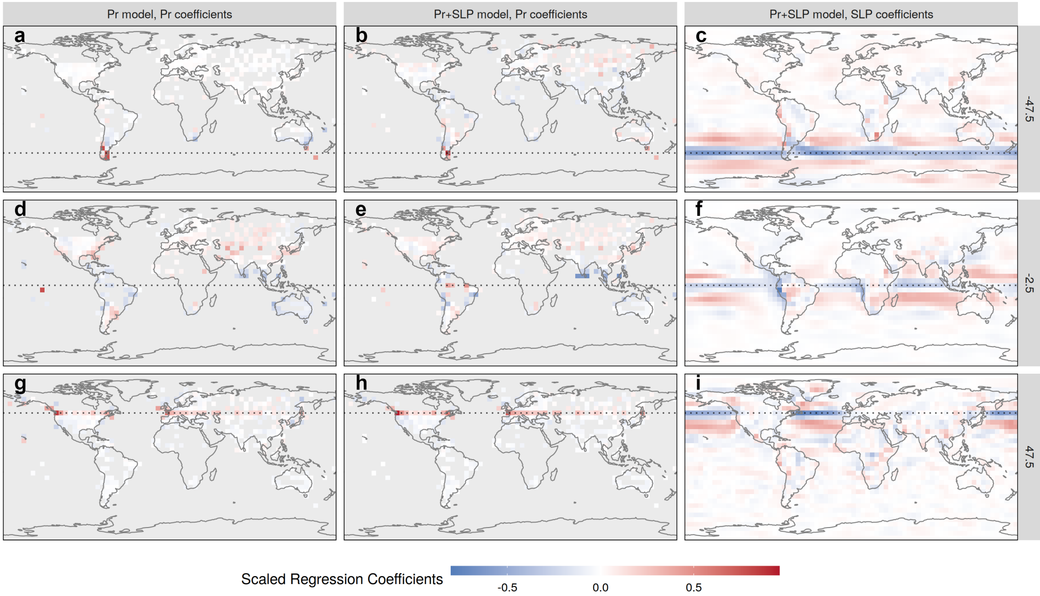

Figure 1. Coefficients of the ridge models trained to predict seasonal DJF precipitation mapped onto their location based on GHCN coverage. The coefficients are scaled by subtracting the mean and dividing by the range from the smallest to largest coefficient for every map respectively. The coefficients are used to predict zonal mean precipitation at -47.5°, -2.5°, or 47.5° from top to bottom. The dashed line indicates the target latitude.

reconstructed time-series are very similar with Pearson correlation values of the reconstructions to the "true" zonal means of 0.63 or higher. To evaluate the performance of the reconstructions for all latitudes we will from now on focus on the Pearson correlation as a summary statistic of how well the reconstructed time series corresponds with the "true" ZMP as simulated by the respective climate model, as shown in Fig. 2 b and c. Both the Pr and Pr+SLP reconstruction approaches show high correlations with the "true" zonal mean in the Northern hemisphere, due to the large number of grid cells available. Pr shows a slightly lower median correlation in the tropics than in the Northern hemisphere in addition to an increased inter-model spread. This decrease in prediction accuracy likely arises due to the limited observational/mask coverage in the tropics but could also be reinforced by model disagreement on tropical precipitation (Pendergrass & Hartmann, 2014). Pr+SLP performs more consistently across all latitudes and displays higher correlation with the true ZMP overall. Interestingly, the model spread is substantially higher in the tropics than in the mid-latitudes, which again could point to model disagreement on tropical precipitation impeding robust prediction of ZMP across models from land precipitation only. The differences between the two model setups, Pr and Pr+SLP, become most apparent in the Southern hemisphere, where the additional coverage from SLP yields the largest performance increase. The Pr model also struggles to reconstruct high latitude precipitation, owing to the lack of observational coverage in those regions. This is remedied in the Pr+SLP model. It is also worth noting that the high latitudes cover less area on the globe, and might thus be subject to higher internal variability.

3.3 Zonal mean precipitation reconstruction with observations

Next, we present the application of the trained models to two different sources of gauge observations, resulting in two reconstructions (GHCN and GPCC). We again dif-

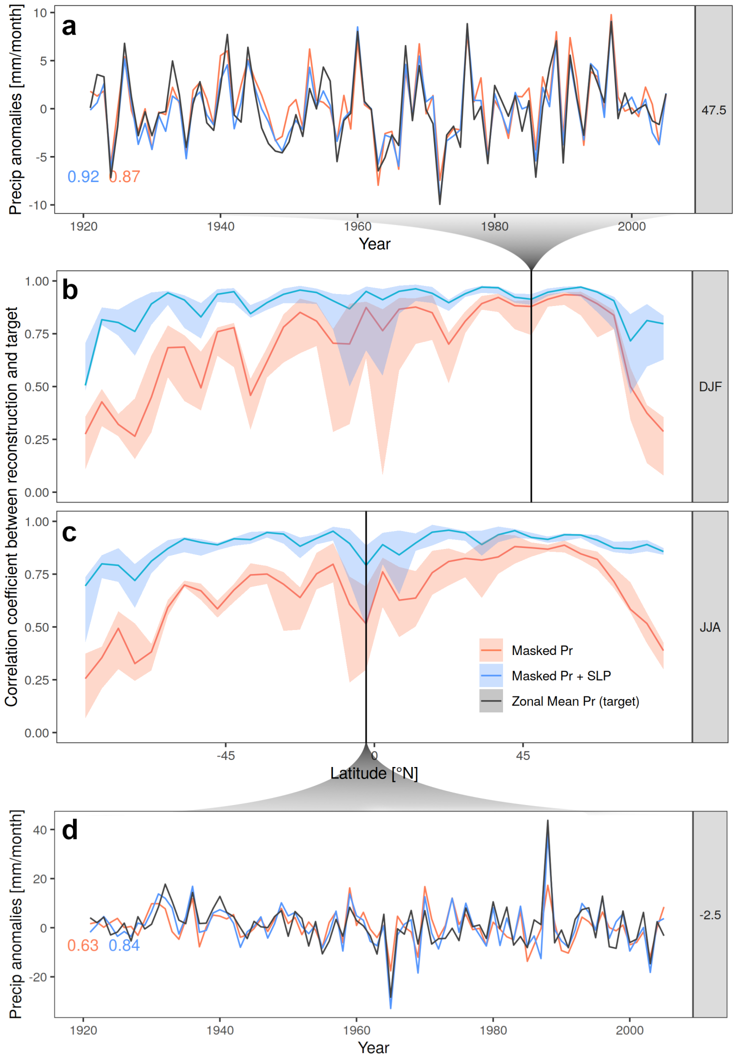

Figure 2. Reconstruction of zonal mean precipitation in the first ensemble member of CESM1-CAM5 at two selected latitudes (a and d). The ridge models use masked precipitation only (Pr) or masked precipitation and unmasked sea level pressure (Pr+SLP) to reconstruct zonal mean precipitation. CESM1-CAM5 model data was excluded from the training. The resulting regression coefficients are then applied to the masked CESM1-CAM5 data. Zonal Mean Pr represents the "true" zonal mean precipitation, calculated from the ensemble member's unmasked data. Plot b and c show the multi-model ensemble average correlation of reconstructions with the "true" zonal mean precipitation of a climate model excluded from training. The thick line represents the median ensemble average correlations and the shading indicates the range from the lowest to the highest ensemble average correlation.

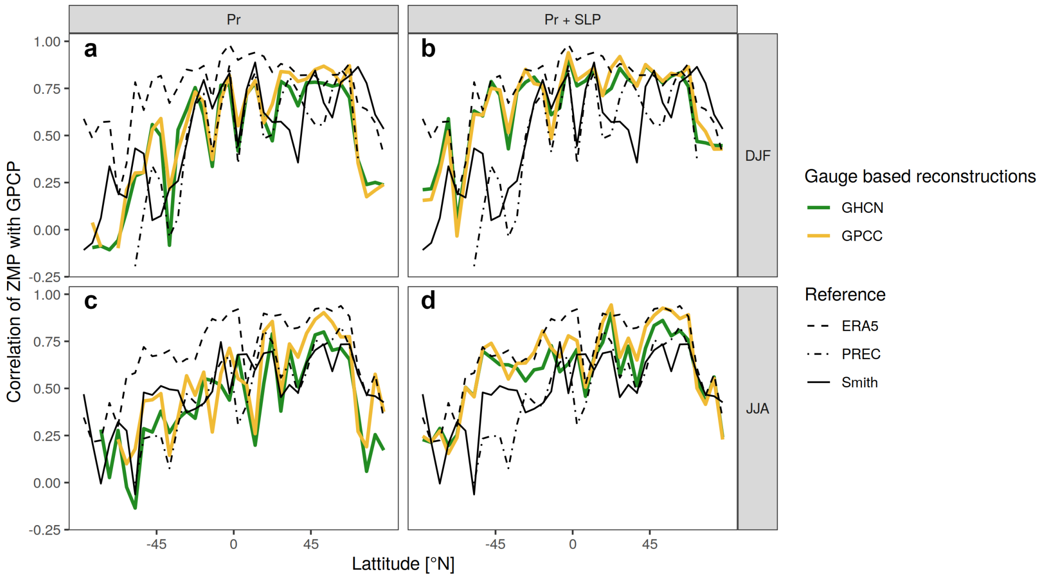

Figure 3. Correlation of observational reconstructions with the satellite based GPCP data from 1979 to 2008. Colors denote the two different rain-gauge data sets used. Subplots a and c are based on only precipitation data (Pr) and b and d based on combining these gauge data sets with reanalysis SLP. Smith and PREC are alternative reconstructions of precipitation and ERA5 is taken from ECMWF's Reanalysis. Note that the black reference lines do not differ between Pr and Pr+SLP.

ferentiate the models trained based on precipitation alone (Pr) and precipitation with the addition of SLP (Pr+SLP). SLP observations come from 20CRv3 in all cases.

The global satellite observations from the Global Precipitation Climatology Project (GPCP) (Adler et al., 2018) serve as the independent verification data set and are assumed to be our most reliable source of global observations. The consistency of our two reconstructions with these "best observations" are assessed by correlating them with ZMP derived from GPCP. To assess the relative performance of our method ZMP derived from three external sources of augmented global precipitation observations – a reconstruction by Smith et al. (2012) (Smith), by NOAA (PREC) (Chen et al., 2002) and ERA5 Reanalysis (ERA5) (Hersbach et al., 2020) – are also correlated with GPCP.

The reconstruction method applied to observations results in accurate estimates of observed ZMP judging from the high correlations with the verification data set GPCP, indicating the method generalizes well from models to observations. Pr performs substantially better in the Northern than in the Southern hemisphere while Pr+SLP shows a smaller difference in correlation between the two hemispheres. Adding the SLP information from 20CRv3 to the ridge reconstruction increases the correlation with GPCP for all latitudes. The biggest impact of using SLP information can again be seen in the Southern hemisphere. The performance of the reconstruction is roughly similar for DJF and JJA.

3.4 Estimating trends in the reconstructions

In the previous subsection, we demonstrated the skill of the historical ZMP reconstructions. Here, we address the possibility of estimating the response of ZMP to external forcing. This follows earlier research that aims to detect forced signals from spatial patterns of climate variables such as temperature or precipitation (Barnes et al., 2019; Sippel et al., 2020), but here we focus on ZMP, which has already been used in attribution studies with satellite data (Marvel & Bonfils, 2013), which were able to detect a signal of external influence in ZMP. They find that expected ZMP changes include increasing precipitation in wet mid latitudes and tropics, and persistence and expansion of dry subtropical regions. We build upon this work, using rain gauge instead of satellite data, to identify trends in ZMP from records starting as early as 1950. We thus calculate linear trends in the previously shown reconstructions (1950-2014) for every latitude from the "Pr + SLP" reconstruction (Figure 4). Trends from the "Pr" reconstruction can be seen in the SI (Figure S2). We additionally apply the masked climate models large ensemble onto the obtained fingerprints and calculate trends for the same time period as for the observations. Additionally, we calculate 65 year trends of unforced pre-industrial control (PiC) data projected onto the fingerprint to reconstruct ZMP in each zonal band.

The trends of the reconstructions show an increase in ZMP in the mid latitudes and the tropics, as well as some decreases in the subtropical latitudes. Only few of the individual latitudes fall outside the range of the possible trends in a pre-industrial simulation. Yet, the pattern across all latitudes shows clear alignment with externally forced climate models: the covariance of the zonal pattern of reconstructed trends with the multi-model mean ZMP trends lies well within the distribution of forced simulations, but would be very unlikely to occur in pre-industrial control simulations for both data sets and both seasons (Figure S3 and S4). The shifts from positive to negative to positive trends between the tropics and the mid-latitudes implies large regions with small trends - which are however still part of the pattern of the response to forcing. The two observational data sets are in general agreement but do display some differences, showing the need for high quality precipitation observations.

4 Conclusions and Outlook

In this paper, we have outlined an approach to reconstruct zonal mean precipitation on a seasonal scale based (1) on land-based precipitation records only, and (2) augmented with reanalyzed SLP. The reconstruction performs very well for the Northern Hemisphere, and especially the addition of SLP produces adequate results for the Tropics and Southern Hemisphere. We have verified the approach by assessing prediction accuracy in a model-as-truth setup, and we have shown that the reconstruction performs well in observations with independent global satellite observations. In the climate model comparison, Pearson correlations are on average around 0.75 and 0.85 for Pr and Pr+SLP reconstructions, respectively, for the tropics and Northern mid-latitudes (but with lower values in the Southern hemisphere). Comparing against satellite data, the reconstructions perform equally well or better to calculating zonal means from existing, alternative precipitation reconstructions (Smith et al., 2012; Chen et al., 2002), and with overall moderately lower skill compared to ERA5 (Hersbach et al., 2020). Our method thus offers a valuable complement for inferring large-scale precipitation metrics.

Human influence on precipitation has long been detected on a global scale (Zhang et al., 2007; Hegerl et al., 2015) but more regional detection and attribution is desirable in order to provide information to policy makers. Our method allows to assess trends in ZMP from station-based data from 1950 onwards, and we identify a strong signal of forced change in the zonal pattern of precipitation. While previous studies have used satellite-based precipitation to detect forced changes in ZMP (Marvel & Bonfils, 2013), our method allows the use of rain-gauge data and further explanatory variables.

Future work could extend the present approach towards estimating regional trends from incomplete observations in various water cycle variables, focusing either on a reconstruction of long-term trends (as illustrated here) or specifically targeting forced or

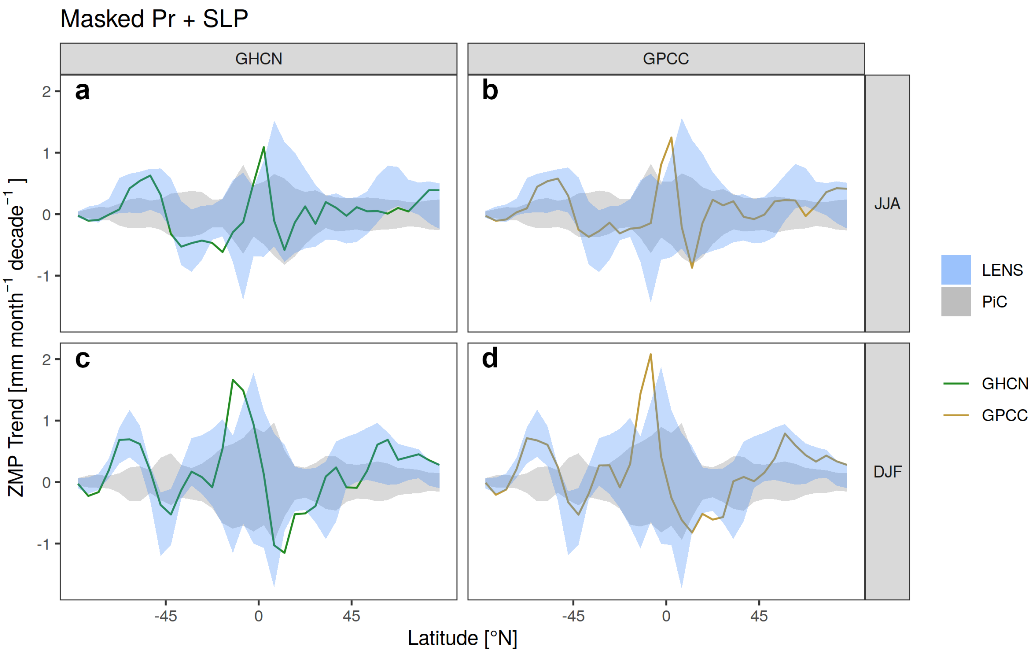

Figure 4. Decadal trends in the reconstructed zonal mean precipitation between 1950 and 2014 based on two different observational data sets GHCN (a and c) and GPCC (b and d) is represented by the thick line. The blue shading indicates the 2.5% to 97.5% quantile range of climate models forced with historical greenhouse gas and aerosol concentration (LENS) from 1950 to 2014. The grey shading indicates 65-year trends in unforced climate models representing pre-industrial conditions (PiC). The reconstructions are based on precipitation and SLP. The panels a and b show the trends during the period of July to August (JJA) and the panels c and d show the respective trends during the months of December to February (DJF).

internal components on a regional scale (Guo et al., 2019; Bonfils et al., 2020; De Vries et al., n.d.), and possibly extended with multivariate predictors or observations

Acknowledgments

We kindly acknowledge the US CLIVAR Working Group for support of the Multi-Model Large Ensemble Archive (MMLEA). We thank the modelling groups listed in Table S1 for making their Large Ensemble simulations available. I.d.V. and S.S. acknowledge funding received from the Swiss National Science Foundation within the project "Combining theory with Big Data? The case of uncertainty in prediction of trends in extreme weather and impacts" (grant no. 167215). S.S. acknowledges funding from the Swiss Data Science Centre within the project "Data Science- informed attribution of changes in the Hydrological cycle" (DASH; C17-01) and within the European Union H2020 project "Artificial intelligence for detection and attribution" (XAIDA; grant no. 101003469).

Open Research Section

Data availability statement

- The Multi-model large ensemble archive used for this study is described by Deser et al. (2020) and can be accessed here:
  `https://www.cesm.ucar.edu/projects/community-projects/MMLEA/`
- The rain gauge observations are taken from the following two sources. GPCC, as described by Schneider et al. (2014), accessible through
  `https://climatedataguide.ucar.edu/climate-data/gpcc-global-precipitation-climatology-centre`
  GHCN, as described in Menne et al. (2018) accessible through
  `https://www.ncei.noaa.gov/products/land-based-station/global-historical-climatology-network-monthly`
- The satellite based precipitation observations (GPCP) are described in Adler et al. (2018) and can be accessed here:
  `https://climatedataguide.ucar.edu/climate-data/gpcp-monthly-global-precipitation-climatology-project`
- We use two reanalysis products.
  ERA5 is described by Hersbach et al. (2020) and is accessible through `https://cds.climate.copernicus.eu/cdsapp#!/dataset/reanalysis-era5-single-levels-monthly-means`
  The 20th Century Reanalysis v3, described by Slivinski et al. (2019), accessible through:
  `https://psl.noaa.gov/data/gridded/data.20thC_ReanV3.html`
- We employ two precipitation reconstructions.
  The first reconstruction is described by Smith et al. (2012), accessible through
  `http://cics.umd.edu/~tsmith/recpr/eof1/full/`
  The second reconstruction is described by Chen et al. (2002), accessible through:
  `https://psl.noaa.gov/data/gridded/data.prec.html`

References

Adler, R. F., Sapiano, M. R. P., Huffman, G. J., Wang, J.-J., Gu, G., Bolvin, D., ... Nelkin, E. (2018). The Global Precipitation Climatology Project (GPCP) monthly analysis (new version 2.3) and a review of 2017 global precipitation. *Atmosphere*, *9*(4), 138.

Bárdossy, A., & Pegram, G. (2014, 11). Infilling missing precipitation records – A comparison of a new copula-based method with other techniques. *Journal of Hydrology*, *519*(PA), 1162–1170. doi: 10.1016/J.JHYDROL.2014.08.025

Barnes, E. A., Hurrell, J. W., Ebert-Uphoff, I., Anderson, C., & Anderson, D.

(2019). Viewing Forced Climate Patterns Through an AI Lens. *Geophysical Research Letters*, *46*(22), 13389–13398. doi: 10.1029/2019GL084944

Berg, A., & McColl, K. A. (2021). No projected global drylands expansion under greenhouse warming. *Nature Climate Change*. Retrieved from `https://doi.org/10.1038/s41558-021-01007-8` doi: 10.1038/s41558-021-01007-8

Bindoff, N. L., Stott, P. A., AchutaRao, K. M., Allen, M. R., Gillett, N., Gutzler, D., ... Jain, S. (2013). Detection and attribution of climate change: from global to regional.

Bonfils, C. J., Santer, B. D., Fyfe, J. C., Marvel, K., Phillips, T. J., & Zimmerman, S. R. (2020, 7). Human influence on joint changes in temperature, rainfall and continental aridity. *Nature Climate Change 2020 10:8*, *10*(8), 726–731. Retrieved from `https://www.nature.com/articles/s41558-020-0821-1` doi: 10.1038/s41558-020-0821-1

Buttlar, J. V., Zscheischler, J., & Mahecha, M. D. (2014, 2). An extended approach for spatiotemporal gapfilling: dealing with large and systematic gaps in geoscientific datasets. *Nonlinear Processes in Geophysics*, *21*(1), 203–215. Retrieved from `www.nonlin-processes-geophys.net/21/203/2014/` doi: 10.5194/NPG-21-203-2014

Chen, M., Xie, P., Janowiak, J. E., & Arkin, P. A. (2002). Global Land Precipitation: A 50-yr Monthly Analysis Based on Gauge Observations. *Journal of Hydrometeorology*, *3*(3), 249–266. Retrieved from `https://journals.ametsoc.org/view/journals/hydr/3/3/1525-7541_2002_003_0249_glpaym_2_0_co_2.xml` doi: 10.1175/1525-7541(2002)003⟨0249:GLPAYM⟩2.0.CO;2

Compo, G. P., Whitaker, J. S., Sardeshmukh, P. D., Matsui, N., Allan, R. J., Yin, X., ... Worley, S. J. (2011, 1). The Twentieth Century Reanalysis Project. *Quarterly Journal of the Royal Meteorological Society*, *137*(654), 1–28. Retrieved from `https://onlinelibrary.wiley.com/doi/full/10.1002/qj.776https://onlinelibrary.wiley.com/doi/abs/10.1002/qj.776https://rmets.onlinelibrary.wiley.com/doi/10.1002/qj.776` doi: 10.1002/QJ.776

Coulibaly, P., & Evora, N. D. (2007, 7). Comparison of neural network methods for infilling missing daily weather records. *Journal of Hydrology*, *341*(1-2), 27–41. doi: 10.1016/J.JHYDROL.2007.04.020

Cowtan, K., Jacobs, P., Thorne, P., & Wilkinson, R. (2018). Statistical analysis of coverage error in simple global temperature estimators. *Dynamics and Statistics of the Climate System*, *3*(1), 1–18. doi: 10.1093/climsys/dzy003

Cowtan, K., & Way, R. G. (2014). Coverage bias in the HadCRUT4 temperature series and its impact on recent temperature trends. *Quarterly Journal of the Royal Meteorological Society*, *140*(683), 1935–1944. doi: 10.1002/qj.2297

Deser, C., Lehner, F., Rodgers, K. B., Ault, T., Delworth, T. L., DiNezio, P. N., ... Ting, M. (2020, 3). Insights from Earth system model initial-condition large ensembles and future prospects. *Nature Climate Change 2020 10:4*, *10*(4), 277–286. Retrieved from `https://www.nature.com/articles/s41558-020-0731-2` doi: 10.1038/s41558-020-0731-2

Deser, C., Phillips, A., Bourdette, V., & Teng, H. (2012). Uncertainty in climate change projections: The role of internal variability. *Climate Dynamics*, *38*(3-4), 527–546. doi: 10.1007/s00382-010-0977-x

De Vries, I., Sippel, S., Pendergrass, A. G., & Knutti, R. (n.d.). *Global detection of forced changes in mean and extreme precipitation is robust but observations disagree on the magnitude of change* (Tech. Rep.).

Gibson, P. B., Chapman, W. E., Altinok, A., Delle Monache, L., DeFlorio, M. J., & Waliser, D. E. (2021, 8). Training machine learning models on climate model output yields skillful interpretable seasonal precipitation forecasts. *Communications Earth & Environment 2021 2:1*, *2*(1), 1–13. Retrieved from `https://www.nature.com/articles/s43247-021-00225-4` doi:

10.1038/s43247-021-00225-4

Guo, R., Deser, C., Terray, L., & Lehner, F. (2019, 3). Human Influence on Winter Precipitation Trends (1921–2015) over North America and Eurasia Revealed by Dynamical Adjustment. *Geophysical Research Letters*, *46*(6), 3426–3434. Retrieved from https://onlinelibrary.wiley.com/doi/full/10.1029/2018GL081316https://onlinelibrary.wiley.com/doi/abs/10.1029/2018GL081316https://agupubs.onlinelibrary.wiley.com/doi/10.1029/2018GL081316 doi: 10.1029/2018GL081316

Hastie, T., & Qian, J. (2014). *Glmnet Vignette.* Retrieved from https://web.stanford.edu/~hastie/glmnet/glmnet_alpha.html

Hegerl, G. C., Catherine, E., Black, L., & Allan, R. P. (2015). Challengest in Quantifying Changes in the Global Water Cycle. *American Meterological Society*(August).

Held, I., & Soden, B. (2006). Robust Responses of the Hydrological Cycle to Global Warming. *Journal of Climate*, *19*(21), 5686–5699. Retrieved from https://journals.ametsoc.org/view/journals/clim/19/21/jcli3990.1.xml doi: 10.1175/JCLI3990.1

Hersbach, H., Bell, B., Berrisford, P., Hirahara, S., Horányi, A., Muñoz-Sabater, J., … Thépaut, J. N. (2020, 7). The ERA5 global reanalysis. *Quarterly Journal of the Royal Meteorological Society*, *146*(730), 1999–2049. Retrieved from https://onlinelibrary.wiley.com/doi/full/10.1002/qj.3803https://onlinelibrary.wiley.com/doi/abs/10.1002/qj.3803https://rmets.onlinelibrary.wiley.com/doi/10.1002/qj.3803 doi: 10.1002/QJ.3803

Hulme, M. (1995, 2). Estimating global changes in precipitation. *Weather*, *50*(2), 34–42. Retrieved from https://doi.org/10.1002/j.1477-8696.1995.tb06074.x doi: https://doi.org/10.1002/j.1477-8696.1995.tb06074.x

Kadow, C., Hall, D. M., & Ulbrich, U. (2020). Artificial intelligence reconstructs missing climate information. *Nature Geoscience*, *13*(6), 408–413. Retrieved from https://doi.org/10.1038/s41561-020-0582-5 doi: 10.1038/s41561-020-0582-5

Kim, J. W., & Pachepsky, Y. A. (2010, 11). Reconstructing missing daily precipitation data using regression trees and artificial neural networks for SWAT streamflow simulation. *Journal of Hydrology*, *394*(3-4), 305–314. doi: 10.1016/J.JHYDROL.2010.09.005

Kondrashov, D., & Ghil, M. (2006, 5). Spatio-temporal filling of missing points in geophysical data sets. *Nonlinear Processes in Geophysics*, *13*(2), 151–159. Retrieved from www.nonlin-processes-geophys.net/13/151/2006/ doi: 10.5194/NPG-13-151-2006

Marvel, K., & Bonfils, C. (2013). Identifying external influences on global precipitation. *Proceedings of the National Academy of Sciences of the United States of America*, *110*(48), 19301–19306. doi: 10.1073/pnas.1314382110

Meehl, G. A., Stocker, T. F., Collins, W. D., Friedlingstein, P., Gaye, A. T., Gregory, J. M., … Zhao, Z. C. (2007). *Global climate projections. Chapter 10.* Retrieved from https://archive.ipcc.ch/publications_and_data/ar4/wg1/en/ch10.html

Menne, M. J., Williams, C. N., Gleason, B. E., Rennie, J. J., & Lawrimore, J. H. (2018). The Global Historical Climatology Network Monthly Temperature Dataset, Version 4. *Journal of Climate*, *31*(24), 9835–9854. Retrieved from https://journals.ametsoc.org/view/journals/clim/31/24/jcli-d-18-0094.1.xml doi: 10.1175/JCLI-D-18-0094.1

Muller, C. J., & O'Gorman, P. A. (2011). An energetic perspective on the regional response of precipitation to climate change. *Nature Climate Change*, *1*(5), 266–271. Retrieved from https://doi.org/10.1038/nclimate1169 doi: 10.1038/nclimate1169

Pendergrass, A. G., & Hartmann, D. L. (2014). Changes in the Distribution of

Rain Frequency and Intensity in Response to Global Warming. *Journal of Climate*, *27*(22), 8372–8383. Retrieved from https://journals.ametsoc.org/view/journals/clim/27/22/jcli-d-14-00183.1.xml doi: 10.1175/JCLI-D-14-00183.1

Salzmann, M. (2016). Global warming without global mean precipitation increase? *Science Advances*, *2*(6), e1501572. Retrieved from http://advances.sciencemag.org/content/2/6/e1501572.abstract doi: 10.1126/sciadv.1501572

Scheff, J., & Frierson, D. (2012). Twenty-First-Century multimodel subtropical precipitation declines are mostly midlatitude shifts. *Journal of Climate*, *25*(12), 4330–4347. doi: 10.1175/JCLI-D-11-00393.1

Schneider, U., Becker, A., Finger, P., Meyer-Christoffer, A., Ziese, M., & Rudolf, B. (2014, 3). GPCC's new land surface precipitation climatology based on quality-controlled in situ data and its role in quantifying the global water cycle. *Theoretical and Applied Climatology*, *115*(1-2), 15–40. Retrieved from https://link.springer.com/article/10.1007/s00704-013-0860-x doi: 10.1007/S00704-013-0860-X/TABLES/3

Shen, S. S., Tafolla, N., Smith, T. M., & Arkin, P. A. (2014, 9). Multivariate Regression Reconstruction and Its Sampling Error for the Quasi-Global Annual Precipitation from 1900 to 2011. *Journal of the Atmospheric Sciences*, *71*(9), 3250–3268. Retrieved from https://journals.ametsoc.org/view/journals/atsc/71/9/jas-d-13-0301.1.xml doi: 10.1175/JAS-D-13-0301.1

Sippel, S., Meinshausen, N., Fischer, E. M., Székely, E., & Knutti, R. (2020). Climate change now detectable from any single day of weather at global scale. *Nature Climate Change*, *10*(1), 35–41. Retrieved from http://dx.doi.org/10.1038/s41558-019-0666-7 doi: 10.1038/s41558-019-0666-7

Slivinski, L. C., Compo, G. P., Whitaker, J. S., Sardeshmukh, P. D., Giese, B. S., McColl, C., … Wyszyński, P. (2019, 10). Towards a more reliable historical reanalysis: Improvements for version 3 of the Twentieth Century Reanalysis system. *Quarterly Journal of the Royal Meteorological Society*, *145*(724), 2876–2908. Retrieved from https://onlinelibrary.wiley.com/doi/full/10.1002/qj.3598https://onlinelibrary.wiley.com/doi/abs/10.1002/qj.3598https://rmets.onlinelibrary.wiley.com/doi/10.1002/qj.3598 doi: 10.1002/QJ.3598

Smith, T. M., Arkin, P. A., Ren, L., & Shen, S. S. P. (2012). Improved Reconstruction of Global Precipitation since 1900. *Journal of Atmospheric and Oceanic Technology*, *29*(10), 1505–1517. Retrieved from https://journals.ametsoc.org/view/journals/atot/29/10/jtech-d-12-00001_1.xml doi: 10.1175/JTECH-D-12-00001.1

Wu, P., Christidis, N., & Stott, P. (2013, 7). Anthropogenic impact on Earth's hydrological cycle. *Nature Climate Change 2013 3:9*, *3*(9), 807–810. Retrieved from https://www.nature.com/articles/nclimate1932 doi: 10.1038/nclimate1932

Zhang, X., Zwiers, F. W., Hegerl, G. C., Lambert, F. H., Gillett, N. P., Solomon, S., … Nozawa, T. (2007, 7). Detection of human influence on twentieth-century precipitation trends. *Nature 2007 448:7152*, *448*(7152), 461–465. Retrieved from https://www.nature.com/articles/nature06025 doi: 10.1038/nature06025